



Optics Letters

Nano-ablation of silica by plasmonic surface wave at low fluence

LEI WANG,¹  XIAO-WEN CAO,¹ MUHAMMAD IRFAN ABID,⁴ QIAN-KUN LI,¹ WEN-JING TIAN,⁵ QI-DAI CHEN,^{1,*} SAULIUS JUODKAZIS,^{2,3}  AND HONG-BO SUN¹

¹State Key Laboratory on Integrated Optoelectronics, College of Electronic Science and Engineering, Jilin University, Changchun 130012, China

²Centre for Micro-Photonics, Faculty of Science, Engineering and Technology, Swinburne University of Technology, Hawthorn, VIC 3122, Australia

³Melbourne Centre for Nanofabrication, ANFF, 151 Wellington Road, Clayton VIC 3168, Australia

⁴Department of Electrical Engineering, Riphah International University, Faisalabad, Pakistan

⁵State Key Laboratory of Supramolecular Structure and Materials, College of Chemistry, Jilin University, Changchun 130012, China

*Corresponding author: chenqd@jlu.edu.cn

Received 1 September 2017; revised 26 September 2017; accepted 26 September 2017; posted 28 September 2017 (Doc. ID 306256); published 25 October 2017

Formation of ripples by ablation of surfaces of laser-irradiated materials is an example of ultrafast energy delivery. Herein, we report on fs-laser optical imprinting of periodic nano-grooves on silica substrate at only 25% of the laser ablation threshold via an interface plasmonic light localization at the ZnS film (top) interface with silica (bottom) by plasmonic surface wave. The nano-grooves were formed throughout ZnS with the same period and orientation imprinted onto the underlying silica. Based on a detailed account of the multi-photon and avalanche ionization using the Drude model, laser-induced plasmonic ablation describes quantitatively the energy deposition from the top ZnS to the substrate of silica. © 2017 Optical Society of America

OCIS codes: (140.3330) Laser damage; (140.3390) Laser materials processing; (320.7110) Ultrafast nonlinear optics; (240.6680) Surface plasmons.

<https://doi.org/10.1364/OL.42.004446>

Femtosecond (fs-) laser-induced periodic surface structures (LIPSS), often referred to as ripples, have increasing interest for their capability of sub-diffraction nanostructuring and richness of laser-matter interaction mechanisms spanning a wide time range [1–4]. Ripples become a general phenomenon observed on nearly all the inorganic [3,4] and some organic materials [3,5]. Two types, the near-subwavelength and deep-subwavelength structures, have been reported [1,6]. The following ultrafast fs-laser processes are key players in energy delivery for ripples' formation: multi-photon ionization [7,8], free carrier absorption (avalanche ionization) [9] plasma formation [10], and harmonic wave generation [11,12]. The final ripple structure is formed by imprinting of the surface wave via longer and complex relaxation and phase transitions back to solid state. Formation of deep-subwavelength structures is attracting the most interest. Research is focused on the evolution of ripples' period and orientation with laser power [6,13], pulse accumulation [6,14,15], laser polarization [16,17],

and spin and angular momenta of photons [18]. Studies are focused on the lateral structure formation defined by polarization of the surface or perpendicular to the incoming laser beam [3,19–21]. The longitudinal structure evolution and nanoscale energy deposition along the propagation of the laser pulse are less explored in terms of control of the energy deposition. The axial extent of the final modification provides control of an optical retardance, which is utilized in polarization optics.

Herein, we report fs-laser optical imprinting of nano-grooves on the substrate of silica via the LIPSS formed on the above-laying film of ZnS. The nano-grooves were found in the continued patterns of the LIPSS formed on the interface between ZnS and silica. The excitation fluence for the groove formation was found in only 25% of the laser ablation threshold of bare silica. A plasmonic nano-ablation model, including self-consistent description of the initial process of carrier excitation, dense e–h plasma time evolution, and the periodic structure formation, was proposed to successfully distinguish the threshold of nano-structuring of ZnS film and under-laying silica. LIPSS are governed by the effective dielectric constant of ZnS created under optical excitation. Laser-induced surface electric enhancement and energy delivery explains the formed nano-ablated grooves on silica substrate.

Near-infrared fs-laser pulses from a Ti:sapphire regenerative amplifier laser system (Spectra Physics) operating at the 800 nm wavelength were used for nano-printing. Pulse duration was 100 fs with a tunable repetition rate that can reach 2.5 kHz. A cylindrical lens with a focal length $f = 35$ mm was used to focus the beam into a linearly shaped focus of 8 mm in length and about 5 μm in width. The sample made of a 100-nm-thick ZnS film sputtered on silica substrate was scanned vertically to the long extension of the focus using a computer controlled step motor driver (Fig. 1). An objective lens of numerical aperture $\text{NA} = 0.7$ and magnification of 50 \times was utilized for determination of the thresholds of ablation. Patterns of ablation dots on ZnS film and the bare silica were fabricated, where the laser fluence was increased gradually to define the threshold

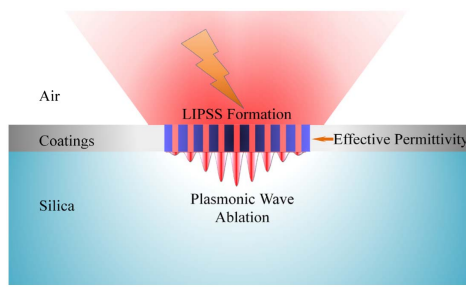


Fig. 1. Mechanism of fs-laser optical imprinting nano-grooves on silica via laser-induced ripples on the ZnS film.

by checking for ablation onset by high-resolution scanning electronic microscopy (SEM, JEOL, 6700F) imaging. The ablation thresholds for single-pulse energy, P , were about 30.2 nJ and 6.9 nJ for silica and ZnS film, respectively. The ablation area S was estimated by $S = \pi(0.61\lambda/\text{NA})^2$. So, the thresholds of ZnS and silica were calculated as P/S at 0.45 J/cm² and 1.98 J/cm², respectively.

Fs-laser optically imprinted ZnS nanostructures are shown in Figs. 2(a) and 2(b) made by cylindrical focusing aligned vertically to the laser polarization direction. Similar laser-induced structures have been observed on ZnS crystal surface [4,22] but less uniform when compared with those structures on a film. Besides, the required pulse number for ablation on ZnS film was larger than that on a crystal [4,22] due to the high transparency of silica (silica is transparent at fluences below its threshold and has no contribution to the light absorption). The structure period was 190 ± 20 nm at the laser fluence 0.5 J/cm² and scanning speed of 10 $\mu\text{m/s}$ (1250 pulses per spot), as shown in [Fig. 2(a)]. On the ZnS-silica interface, nano-grooves were found imprinted below ZnS gratings, as shown in Fig. 2(b) at 0.6 J/cm² (scanning speed 10 $\mu\text{m/s}$). By immersion of the sample into H₂SO₄ (pH \approx 1) for 30 s after structuring, the remaining ZnS was removed together with LIPSS pattern in it. Ripples printed on the inner ZnS-silica interface had proven that the nano-grooves were deeply imprinted into the ZnS and were present throughout the entire

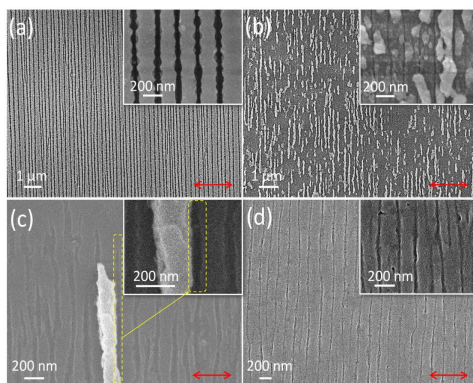


Fig. 2. Deep-subwavelength nanostructures on ZnS film and the corresponding nano-grooves formed on both sides of the ZnS film. (a) Nanostructures induced on ZnS at 0.5 J/cm². (b) Nanostructures and nano-grooves on/in ZnS at 0.6 J/cm². (c) Nano-grooves on silica at the speed of 20 $\mu\text{m/s}$ after H₂SO₄ washing for 30 s. (d) Silica nano-grooves at the speed of 10 $\mu\text{m/s}$ after removing all the ZnS. Scale bars are 200 nm. Polarization of fs-laser field is denoted by arrows.

thickness of ZnS [regions highlighted in dashed boxes in Fig. 2(c)] and in the silica [Figs. 2(c) and 2(d)]. The silica nano-grooves were strongly dependent on the scanning speed and become irregular when the scanning speed is above 20 $\mu\text{m/s}$ [625 pulses per spot; Fig. 2(c)]. Light intensity is also another factor in the nano-groove formation by influencing the ablation of ZnS nanogratings. Periodic nano-grooves were observed on the substrate, as shown in Fig. 2(d) by etching out the ZnS gratings shown in Fig. 2(a). But when the laser fluence was more than 0.7 J/cm², nano-grooves could not be found because an entire ZnS film was ablated first. Also, there are no nanostructures imprinted on silica when the film thickness was larger than 200 nm.

Since nano-grooves were perpendicular to the laser polarization, 2D patterns of nanostructures were obtained by two crisscross exposures, as shown in Figs. 3(a) and 3(b). By cylindrical lens scanning, periodic ZnS nanostructures on silica over an area of 8 mm \times 10 mm have been fabricated. By dip-wet etching in H₂SO₄ (pH \approx 1, 30 s) to remove the ZnS film, nano-grooves over a large area were obtained and analyzed by atomic force microscopy (AFM; iCON, Veeco), as shown in Fig. 3(c). The depth measured from an area of approximately 20 periods was observed around 10 nm. Such nano-grooves were found to be more localized as compared with ripples directly induced by the fs laser on the surface of bulk materials. By scanning a cylindrically focused fs-laser beam, large-area nano-grooves can be nano-ablated/printed on bare silica at a power density of about 25% from the threshold of ablation of the silica surface [Fig. 2(b)]. All the structures shown in Figs. 3(a)–3(c) were fabricated under a power density of 0.5 J/cm² and scanning speed of 10 $\mu\text{m/s}$. The period of nano-grooves on silica was deep-subwavelength and did not obey the predictions by Sipe's model of interaction between the incident light and scattered surface waves [23]. Since the period of nano-grooves was the same as the nano-gratings on ZnS, the model based on second-harmonic generation (SHG) [12] and diffraction is not applicable either. The fs-laser-induced plasmonic excitation is presented here to account for the periodic nanostructure formation on the silica below the laser breakdown threshold.

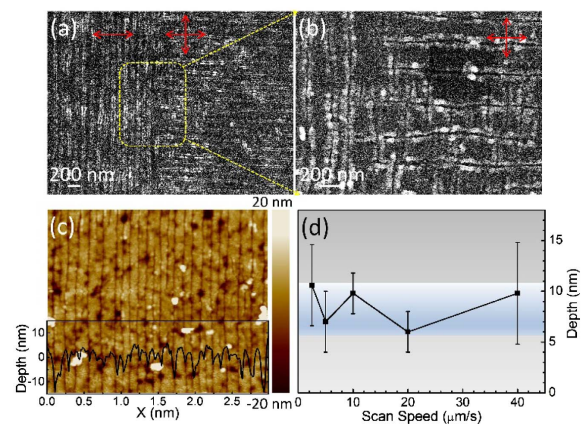


Fig. 3. (a) and (b) Two-dimensional pattern of nano-grooves formed by crisscross scanning of sample surface. (c) AFM image of nano-grooves on silica. (d) Depth for grooves at different scan speeds. Scale bars denote 200 nm. Polarization of fs-laser field is denoted by arrows.

Instantaneous optical absorption is the first process of laser-matter interaction determined by the photon energy and the bandgap of the material. The nonlinear character of this interaction is captured for the laser wavelength of 800 nm (1.55 eV), which corresponds to at least three-photon absorption (3PA) for electronics transition from the valance to conduction band in ZnS film with a bandgap of 3.35 eV, while a six-photon absorption (6PA) would be required for silica (the bandgap ~ 8.0 eV). Nonlinear ionization generates electrons by two major mechanisms: via multi-photon ionization (MPI) and avalanche or impact ionization (IMP). The electron generation rate can be calculated by the following formulas for ZnS film and silica [7]:

$$\frac{dn_e}{dt} = n_e \omega_{\text{imp}} + n_a \omega_{\text{mpi}}, \quad (1)$$

$$\omega_{\text{imp}} \approx \frac{\epsilon_{\text{osc}}}{J_i} \left(\frac{2\omega_0^2 \nu_{\text{eff}}}{\omega_0^2 + \nu_{\text{eff}}^2} \right), \quad (2)$$

$$\omega_{\text{mpi}} \approx \omega_0 n_{\text{ph}}^{3/2} \left(1.36 \frac{\epsilon_{\text{osc}}}{J_i} \right), \quad (3)$$

$$\epsilon_{\text{osc}} = (1 + \alpha^2) \frac{e^2 E^2}{4m\omega_0^2}, \quad (4)$$

where n_e is the electron density, n_a is the density of neutral atoms, w_{imp} is the time-independent probability for the ionization by electron impact and w_{mpi} is the probability for the MPI, n_{ph} is the number of multi-photon absorption, J_i is the ionization potential (the energy gap), $\nu_{\text{eff}} = 1/\tau_D$ is the effective collision frequency, and τ_D is the effective collision time.

Considering the relationship of electric field E and intensity [7], $I = I_0 e^{-t/\tau^2}$ and the measured fluence $F = F_0 \int_{-\infty}^{+\infty} I dt$, one can get the expression for E :

$$E = \sqrt{\frac{2F_0}{\sqrt{\pi} c \tau_0 \epsilon_0 \sqrt{\epsilon}}} \quad (5)$$

where τ is the pulse duration, ϵ_0 is the vacuum permittivity, ϵ is the dielectric constant, and c is the speed of light in vacuum.

By using the iterative method implemented with MATLAB code with the ansatz above, the time evolution of the excited carrier concentration could be derived as

$$n_e^{(i)} = n_e^{(i-1)} + [n_e^{(i-1)} \omega_{\text{imp}} + n_a \omega_{\text{mpi}}] \Delta t, \quad (6)$$

where $n_e^{(0)} = n_0$, $\Delta t = \tau/N$; $n_e^{(i)}$ is the i^{th} calculation of n_e at the time of $i \times \Delta t$ in one cycle of τ ; and $N = 300$ is the number of iterative steps. By iterative calculations considering the temporal Gaussian light intensity, a temporal density evolution of e-h plasma N_e was calculated considering the *in situ* changing reflectivity derived by the formulas presented below [Fig. 4(a)]. Plasma density increased fast and exceeded the critical plasma density N_c , which is generally accepted as the threshold of an optical breakdown [7]:

$$N_c(\lambda) = \frac{\epsilon_0 m_e \omega_0^2}{e^2} \frac{1.1 \times 10^{21}}{\lambda[\mu\text{m}]}. \quad (7)$$

The measured threshold of power density at ablation for the ZnS film and silica was a little bit higher than that calculated by the critical plasma density, 0.41 J/cm^2 and 1.8 J/cm^2 ,

respectively. Reflection due to the carrier excitation shown in Fig. 4(a) was taken into account for the used iterative method to provide self-consistent temporal evolution of plasma density. Reflectivity, R , follows directly from the Drude model and dielectric function [22]:

$$\omega_p = \sqrt{\frac{N_e e^2}{\epsilon_0 m^*}}, \quad (8)$$

$$\epsilon^* = 1 + \frac{n_e - n_0}{n_0} (\epsilon_n - 1) - \frac{\omega_p^2}{\omega_0^2} \left(\frac{1}{1 - \omega_0 \tau_D^{-1}} \right), \quad (9)$$

$$R = \frac{(n-1)^2 + k^2}{(n+1)^2 + k^2}, \quad (10)$$

where $(n + ik)$ defines the real and imaginary parts of the refractive index; R is the surface reflection; and $\delta_{\text{sp}} = c/2wk$ defines the skin depth for ZnS, $\delta_{\text{sp}}(\text{ZnS})$, and the substrate of silica, $\delta_{\text{sp}}(\text{Silica})$.

As shown in Fig. 3(b), the dielectric constant of ZnS film becomes a metal-like material to support the surface plasmon polariton (SPP) wave. The wavenumber of the plasmonic wave is defined by Eq. (11) [22]:

$$k_{\text{sp}} = k \sqrt{\frac{\epsilon_d \epsilon^*}{\epsilon_d + \epsilon^*}}. \quad (11)$$

The period of ripples on ZnS can be described by the following equation [depicted in Fig. 4(b)]:

$$\Lambda = \frac{\lambda_{\text{sp}}}{2} = \frac{\pi}{\text{real}(k_{\text{sp}})}. \quad (12)$$

In experiments, the period of $190 \pm 20 \text{ nm}$ was observed [Fig. 4(b)], which is consistent with earlier observed actions [22].

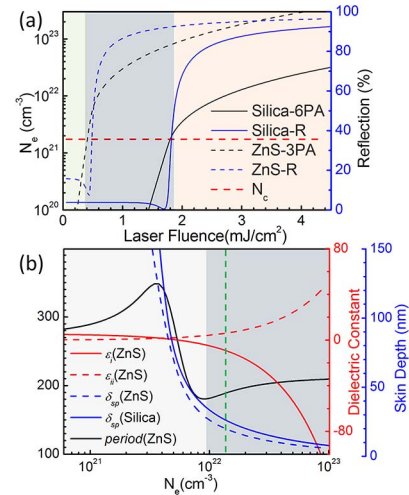


Fig. 4. Plasma density evolution and LIPSS period for ZnS nano-gratings. (a) Plasma electron density in ZnS film and silica substrate versus laser fluence following Eqs. (1)–(6) for the MPI and IMP. The light blue and light red areas represent a parameter space of over-critical plasmas for ZnS and silica, respectively. (b) Period of surface plasmon polariton (SPP), the dielectric constant, and skin depth at different plasma densities for ZnS film. The green line represents the parameters for the period of 190 nm.

As shown in Fig. 4(a), most of the light energy was used for electron excitation and would then be reflected by the formed plasma layer whose reflectivity increased with the excitation. These two counteracting processes built up a balance for the stable deep-subwavelength structure formation. However, the skin depth of ZnS was less than 50 nm and limited the energy deposition depth, which hampers generation of the deep nano-grooves.

Once ripples on ZnS were formed, a light enhancement arose in the openings of the grooves, as shown in Fig. 5. The $|E/E_0|^2$ is around 1 in the case of non-excited structures with a refractive index of ZnS, while for the dielectric constant of the structures with a metal-like dielectric permittivity (at $N_e = 1.426 \times 10^{22} \text{ cm}^{-3}$), the enhancement, $|E/E_0|^2$, reached more than 30 times. The energy deposition is dynamically transported from the interface with air through the ZnS film to the interface with silica in the presence of grooves, as shown in temporal snap shots in Figs. 5(d)–5(f). The beginning entrance (at about 3.6 fs), the middle of the ZnS layer (3.75 fs), and the end (3.9 fs) are shown in Visualization 1 of the supporting material sections. A stable enhancement with factor >5 times is shown in Figs. 5(b) and 5(c), which would reach the threshold of silica ablation and result in the nano-groove formation. The depth of energy deposition is affected by the skin depth, which is around 10 nm, as in experimental results. Light field enhancement was simulated using finite difference time domain (FDTD) method (Lumerical) for the grating pattern [Figs. 5(a)–5(c)]. The dielectric constant of excited ZnS was taken as $\epsilon_i + i\epsilon_{ii} = -12.607 + i*7.366$ at a period of 190 nm, shown as the green line in Fig. 4(b). Film thickness was set as that in the experiment, 100 nm.

In summary, periodic nano-grooves have been nano-printed on silica substrate at 25% of the laser damage threshold via laser-induced periodic structures made on the ZnS film. The observation was modeled via plasmonic excitation and provides a good quantitative matching. The self-consistent light absorption during the laser pulse and a fast-changing reflectivity were calculated iteratively considering the MPI and IMP plasma

generation pathways using the Drude model. The model accounts for the temporal evolution of the carrier concentration and deep-subwavelength structure imprint. The thresholds of ZnS and silica ablation, period of LIPSS on ZnS, and their period make a satisfactory match with the experiment. Although not detailed here, the same phenomenon also has been observed on glass substrate through an indium tin oxide (ITO) layer. The observed phenomenon is generic for semiconductors and transparent dielectric and provides the control for nanoscale structuring/printing.

Funding. National Key R&D Program of China (2017YFB1104600); National Natural Science Foundation of China (NSFC) (91423102, 61590930, 91323301, 61435005).

Acknowledgment. We thank the Optics Laboratory for the use of its equipment. S. J. is grateful for the Changjiang professorship project at Jilin University.

REFERENCES

- R. Buividas, M. Mikutis, and S. Juodkazis, *Prog. Quantum Electron.* **38**, 119 (2014).
- K. Sugioka and Y. Cheng, *Light Sci. Appl.* **3**, e149 (2014).
- J. Bonse, S. Höhm, S. V. Kirner, A. Rosenfeld, and J. Krüger, *IEEE J. Sel. Top. Quantum Electron.* **23**, 109 (2017).
- L. Wang, Q.-D. Chen, X.-W. Cao, R. Buividas, X. Wang, S. Juodkazis, and H.-B. Sun, *Light Sci. Appl.* **6**, e17112 (2017).
- Á. Rodríguez-Rodríguez, E. Rebollar, M. Soccio, T. A. Ezquerro, D. R. Rueda, J. V. Garciaamos, M. Castillejo, and M. C. Garciagutierrez, *Macromolecules* **48**, 4024 (2015).
- L. Wang, B.-B. Xu, X.-W. Cao, Q.-K. Li, W.-J. Tian, Q.-D. Chen, S. Juodkazis, and H.-B. Sun, *Optica* **4**, 637 (2017).
- S. Juodkazis, A. V. Rode, E. G. Gamaly, S. Matsuo, and H. Misawa, *Appl. Phys. B* **77**, 361 (2003).
- M. Malinauskas, A. Zukauskas, G. Bickaikaite, R. Gadonas, and S. Juodkazis, *Opt. Express* **18**, 10209 (2010).
- B. Rethfeld, *Phys. Rev. Lett.* **92**, 187401 (2004).
- R. R. Gattass and E. Mazur, *Nat. Photonics* **2**, 219 (2008).
- A. Borowiec and H. K. Haugen, *Appl. Phys. Lett.* **82**, 4462 (2003).
- X.-F. Li, C.-Y. Zhang, H. Li, Q.-F. Dai, S. Lan, and S.-L. Tie, *Opt. Express* **22**, 28086 (2014).
- Y. Miyasaka, M. Hashida, T. Nishii, S. Inoue, and S. Sakabe, *Appl. Phys. Lett.* **106**, 013101 (2015).
- S. Hohm, A. Rosenfeld, J. Kruger, and J. Bonse, *J. Appl. Phys.* **112**, 014901 (2012).
- R. Buividas, S. Rekštytė, M. Malinauskas, and S. Juodkazis, *Opt. Mater. Express* **3**, 1674 (2013).
- R. D. Murphy, B. Torralva, D. P. Adams, and S. M. Yalisove, *Appl. Phys. Lett.* **104**, 231117 (2014).
- S. Gräf and F. A. Müller, *Appl. Surf. Sci.* **331**, 150 (2015).
- C. Hnatovsky, D. Grobnc, D. Coulas, M. Barnes, and S. J. Mihailov, *Opt. Lett.* **42**, 399 (2017).
- Y. Liao, J. Ni, L. Qiao, M. Huang, Y. Bellouard, K. Sugioka, and Y. Cheng, *Optica* **2**, 329 (2015).
- D. Tan, K. N. Sharafudeen, Y. Yue, and J. Qiu, *Prog. Mater. Sci.* **76**, 154 (2016).
- M. Malinauskas, A. Zukauskas, S. Hasegawa, Y. Hayasaki, V. Mizeikis, R. Buividas, and S. Juodkazis, *Light Sci. Appl.* **5**, e16133 (2016).
- L. Wang, Q.-D. Chen, R. Yang, B.-B. Xu, H.-Y. Wang, H. Yang, C.-S. Huo, H.-B. Sun, and H.-L. Tu, *Appl. Phys. Lett.* **104**, 031904 (2014).
- J. F. Young, J. S. Preston, H. M. van Driel, and J. E. Sipe, *Phys. Rev. B* **27**, 1155 (1983).

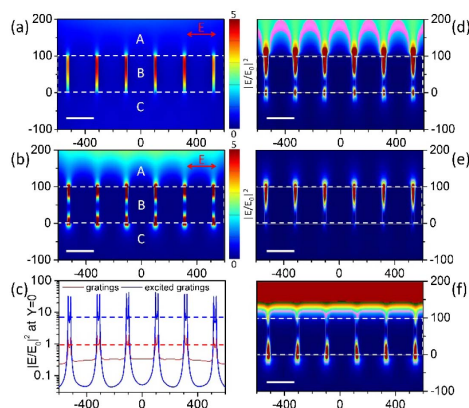


Fig. 5. Light intensity enhancement and energy deposition for the formation of nano-grooves on silica. A grating pattern on ZnS (a) and ZnS with pre-formed ablation grooves photo-excited (b) at the same conditions as in (a). The curve in (c) shows the light intensity enhancement on the interface of ZnS nanogratings and silica; A, B, and C denote the air, ZnS nano-gratings, and silica, respectively. (d)–(f) show the instant changing of light intensity as time increasing after light irradiation (Visualization 1).